Ibn Al-Haitham Journal for Pure and Applied Sciences
Journal homepage: jih.uobaghdad.edu.iq
PISSN: 1609-4042, EISSN: 2521-3407
IHJPAS. 2025, 38(3)

Analysis of the Electrical Conductivity Mechanisms and Energy Density of States in Ternary Chalcogenide Alloy S_{60}-Se_{40-X}-Pb_X

Mohamed M. Ghazi[1*] and Kareem Ali Jasim[2]
[1,2] Department of Physics, College of Education for Pure Science (Ibn Al-Haitham), University of Baghdad, Baghdad, Iraq.
[*]Corresponding author.

Received: 14 September 2024 Accepted: 1 December 2024 Published: 20 July 2025
doi.org/10.30526/38.3.4035

Abstract

We studied in this investigation the changes of the continuous conductivity of the electricity ($\sigma_{d.c}$) due to substituting part of Selenium with Lead in an S_{60}-Se_{40-X}-Pb_X alloy at weight ratios x = 0, 10, 20, and 30. Our investigation includes an examination of $\sigma_{d.c.}$ mechanisms in chalcogenide semiconductors and governing the equations of the continuous D.C. electrical conductivity, and the application of these measured characteristics of S_{60}-Se_{40-X}-Pb_X glasses to assess Lead's impact on extended, local, and Fermi energy state densities. Some procedures were applied to the materials, such as mixing, grinding, heating in quartz ampoules, placing them in a furnace, and heating them at 360°C. The results showed that electrical conduction occurs in three modes (conduction at high temperatures in the extended state, conduction at moderate temperatures in the local state, and conduction at low temperatures in the variable range hopping (VRH).

Keywords: D.C conductivity, Density, Fermi states, Tail width, Chalcogenide, Hopping distance.

1. Introduction

The researchers in the electronics field have developed this industry field and also created research and experiments; they have improved the effectiveness of the materials used in this industry and reduced the cost and the size of the products (1). Researchers also focus on analyzing the material properties of amorphous and random materials and using them as alternatives to crystalline materials, as they can be produced by introducing certain impurities and improving their electrical conductivity. Chalcogenides are currently considered materials of interest due to their many technological applications (for example, solar cells, energy applications, light emission applications, and high-frequency amplifiers) (2, 3). Research has revealed that compounds containing lead, lithium, and bismuth can change the conductivity of molten glass and can also convert the cation type from N to P type in chalcogen semiconductor materials (4).

Chalcogenides were originally advanced for testing and applications in semiconductor devices as early as the 1950s. The chalcogenide semiconductor science displays a wide

soluble ingot spectrum and a wider band gap device that approaches the ideal energy band gap. Controlling the proportion of (Tellurium, Selenium, and Sulfur) allows you to tailor the electronic characteristics of these alloys. The chalcogenide semiconducting ingots are favorable nominees due to the small band gap (1.0–1.6 eV) and increased solar spectrum extinction factor in the visible region. An electron undergoes numerous transitions in the extended and localized state of an amorphous semiconductor, Movement caused by diffusion and drift in D.C. electric fields, and absorption-emission (5). The objective of this study is to produce an alloy called S60-Se40-X-PbX with varying concentrations of Pb (0, 10, 20, and 30) using the solid-state reaction method.

The D.C electrical conductivity changes in the ternary chalcogenide alloy S60-Se40-X-PbX, resulting from the partial replacement of selenium with lead at different weight ratios (x = 0, 10, 20, and 30) were studied. The conduction mechanisms in the semiconductor were explored and the equations controlling the electrical conductivity were applied. These results were used to determine the effect of adding lead to the chalcogenide alloy and its change in the properties of the density in the three states of energy of the alloy (extended, local, and Fermi level).

2. Materials and Methods

2.1. The Theory part

Temperature-dependent electrical conductivity is one of the tools used to investigate the conduction mechanisms in various materials. Moti and Davis controlled the conduction of electronic semiconductors with an amorphous state by three mechanisms: conduction at high temperatures in extended states, conduction at moderate temperatures in localized states, and conduction at low temperatures by hopping in a variable range. They found that the analysis of electronic transport data affects the distribution of energy state densities (6). At low temperatures, conductivity between the localized energy states near the Fermi level involves either an electron or a hole. through the local energy state levels at the energy band tails with moderate temperatures, the conductivity will be facilitated, where charge transfer occurs through hops between these local levels. Conversely, at high temperatures, electrical conductivity primarily takes place between extended energy state levels. The mobility within the extended state surpasses that of the local state, making high-temperature conductive measurements preferable (7). This discussion will explore the detailed equations describing the three types of DC conductivity in the extended, localized, and Fermi levels. In these regions, these equations will assist in calculating the width of these bands and determining their density of states. The D.C conductivity can be represented in chalcogenide with the following equation (8):

$$\sigma = \sigma_{01} e^{(-\frac{E_1}{KT})} + \sigma_{02} e^{(-\frac{E_2}{KT})} + \sigma_{03} e^{(-\frac{E_3}{KT})} \quad (1)$$

Below are the equations for electron conduction; however, analogous equations for hole conduction can be formulated. These three terms correspond to distinct conduction mechanisms and will be addressed individually.

2.2. The region of elevated temperatures

In the beginning section, the main process entails band conduction via extended states. This domain is denoted by the initial component in the first equation (9). The extended states are preferred by the carriers of charge, resulting in an activation energy E_1 by $E_F - E_V$.

$$\sigma = \sigma_{01} e^{(-\frac{E_1}{KT})} \quad (2)$$

σ_{01} is the factor of pre-exponential, E_c-E_f is the energy of activation (eV), while T denotes the temperature in Kelvin. By applying the logarithm to both sides:

$$\ln \sigma = \ln \sigma_{01} - \frac{E_1}{KT} \quad (3)$$

Hence, the gap of energy will be ascertained by the subsequent equation once the slope value has been computed (9):

$$E_1 = (E_C - E_F) = \frac{\ln \sigma}{K_B T} \quad (4)$$

$$\sigma_0 = eN(E_C)KTU_C \quad (5)$$

U denotes the charge displacement, and the density at the extended state is represented by $N(E_c)$ (9).

$$U_C = \frac{eD}{KT} \quad (6)$$

Upon substituting the value of U into equation 5, the formula evolves into the subsequent equation, with D representing the diffusion coefficient.

$$\sigma_0 = e^2 N(E_C) D \quad (7)$$

Once D's value is factored into equation 7, where we got it from D equals 1/6 Ve a2, it adopts the subsequent formula (9):

$$\sigma_{0ext.} = (\frac{1}{6}) e^2 a^2 V_e N(E_C) \quad (8)$$

The distance between interatomic is $\mathbf{a} = 0.026 \frac{e^2}{\hbar \sigma o}$, the frequency of electrons can be described by the equation $\text{Ve} = \frac{\hbar}{a^2 M}$

$$N(E_{ext}) = [\frac{6m}{e^2 \hbar}] \sigma_{0ext} \quad (9)$$

The black arrow in **Figure (1)** symbolizes the excitation process. It will be elaborated upon later that the energy gap is temperature-dependent. Therefore, the activated energy denoted by σ requires adjustment through temperature correction.

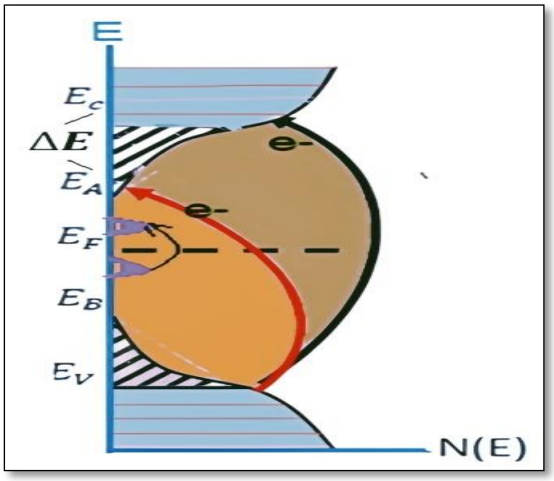

Figure 1. Illustrates a comparison between two scenarios: extended conduction entails the elevation of an electron into the band of conduction followed by movement of the variable range near the edge level bands.

2.3. The conduction by hopping via the states of localized

This operational mode, manifesting at reduced temperatures, is coined as local state conduction. Within this context, through tunneling in unoccupied levels of neighboring centers, the conductivity stems. It encompasses the migration of the carriers of electron or hole charges towards the band's periphery and its local states, succeeded by a hopping mechanism. The energy of activation for this conductivity will be denoted by $E_2=E_F - E_B + w_1$, and the energy of activation will be represented by w_1 and is crucial for transitions between local states (10):

$$\sigma = \sigma_{02} e^{(-\frac{E_A - E_F + W_1}{KT})} \quad (10)$$

$$\sigma_{01} = (\frac{1}{6}) e^2 R^2 V_{ph} N(E_{loc}) \quad (11)$$

Where the frequency of phonon is represented by V_{ph} and the hopping distance is represented by R and it is between any two localized states.

$$N(E_{loc}) = [\frac{6}{e^2 V_{ph} R^2}] \sigma_{0loc} \quad (12)$$

$$\text{So, } R = 0.7736 [\frac{\Delta E a^{-1}}{N(E_C)(KT)^2}]^{0.25} \quad (13)$$

E_1-E_2=ΔE represents the width of tail- energy is illustrated in **Figure (1)**, where the optical absorption coefficient is represented by α^{-1} and its value 10^{-7} cm. The red arrow in **Figure (1)** depicts the excitation process. (11-13).

2.4. The conduction by hopping via the states of localized

As outlined below, the third mechanism of conduction, prominent at extremely low temperatures, is known as VRH. This mode entails conduction by charge carriers within defects close to E_f by tunnel assisted hopping (12):

$$\sigma = \sigma_{03} e^{(-\frac{B}{T^{\frac{1}{4}}})} \quad (14)$$

According to Mott and Davis's analysis of the hopping by the variable range, conductivity transitions into a near-perfect conduction mechanism. Close to the level of Fermi and when the defects are positioned at this level, the conductivity by (VRH) is defined by equation (3) and with the following equation that represents the B exponential term (14):

$$B = 2(\frac{\alpha^3}{k_B N(E_F)})^{\frac{1}{4}} \quad (15)$$

$$N(E_F) = \frac{16\alpha^3}{B^4 KT} \quad (16)$$

$$\sigma_{03} = (\frac{1}{6}) e^2 V_{ph} R^2 N(E_F) \quad (17)$$

$$R = [\frac{9}{(8\pi\alpha N(E_F) k_B KT)}]^{-\frac{1}{4}} \quad (18)$$

The density of states close to the Fermi level is $N(E_F)$, while the localization length of the gap states is α^{-1} and is assumed to be (10-7) cm. k_B refers to the Boltzmann constant in electron-volts/K at temperature T which is calculated at the hopping. B was calculated to provide measurements that enable us to approximate the density of defects inside the gap. (selected as 80 K for these computations). Consequently, the activation energy W necessary for electron traversal near the Fermi level at low temperatures is derived from:

$$W = \frac{3}{(4\pi R^3 N(E_F)} \quad (19)$$

Defects situated near the midpoint of the gap, like dangling bonds, serve as the source of carriers in Variable Range Hopping (VRH). Thus, through this method, we can observe what happens in crystalline semiconductors. As for the case of electrical conduction in non-crystalline semiconductors, the researchers proposed three processes for electrical conduction according to the temperature range that is imposed on random semiconductors. The first region is at high temperatures, in which conduction occurs due to the extended energy state levels, while in the second region, the temperature is moderate and thus facilitates the process of electrical conduction through the local energy state levels and at their edges. As for the last region, in which the temperature is low, electrical conduction occurs through the jumping of electrons or their transfer between the objective energy states and near the Fermi level (13).

2.5. Experimental part

High-purity S, Se, and Pb (99.9%) were obtained for this purpose from BDH Chemical Ltd, Poole, England. To measure proper weights, we used a sensitive electronic balance. When

using the sensitive electronic balance in the laboratory, it should be cleaned from the inside and outside. It is preferable to use the same balance throughout the preparation of the samples to avoid errors. This type of scale can determine the weights with high accuracy. The alloy elements were weighed on this sensitive scale based on the atomic weight ratio.

These chemical components were then ground in an electric grinder for 30 minutes. Next, the fine powder was compressed to form samples with a diameter of 1.5 cm by applying a load of approximately 5 tons using a hydraulic compact (hydraulic uniaxial press), and forming samples with a thickness of 0.3 cm. To prevent the reactions at higher temperatures between the sample components and oxygen, we used quartz ampoules and placed the samples in there, evacuated and heated them in a furnace at a rate of 5 K/min until they reached a temperature of 360°C with sealed them under a vacuum of 10-3, non-vacuum electric Carbonite furnace, at the furnace is an electrical device with thermal insulation temperature controlled by a thermal regulator and is used for the process of drying, heating, sintering and calcification, temperature range ranging from (25-1100) °C. The temperature was maintained at 360°C for three hours.

Then the resulting vitreous material was crushed, and then it was removed from the quartz ampoules. then the molten sample was further crushed using a slurry for thirty minutes, followed by crushing with a hydraulic press to five tons to create disc-shaped samples. The following chemical formulas represent these samples: S60-Se40 for x = 0, S60-Se30-Pb10 for x = 10, S60-Se20-Pb20 for x = 20, and S60-Se10-Pb30 for x = 30. As a function of the temperature, we calculate the parameters of electrical current and voltage, and then the DC electrical conductivity of these samples.

3. Results and Discussion

The $\sigma_{d.c}$ was assessed at various temperatures. The relationship in **Figure (2)**, between $\sigma_{d.c}$ and temperature are illustrated for the S_{60}-Se_{40-X}-Pb_X glass systems (x = 0, 10, 20, and 30). It is noticeable from these graphs that each curve (for each x value) exhibits three distinct regions. based on the slope of each four curves and their three regions respectively, the activation of energy was determined, as detailed in **Table (1).**

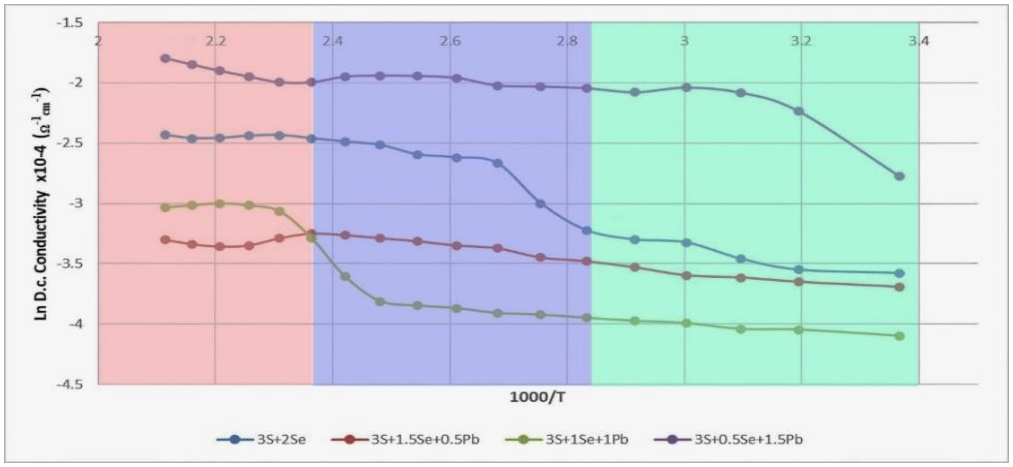

Figure 2. Illustrates the conductivity (σ_{dc}) with respect to temperature for the S_{60}-Se_{40-X}-Pb_X glass compositions varying x (0, 10, 20, and 30).

Table 1. Displays the composition-dependent activation energies and σ_0 for three different states of regents in S_{60}-Se_{40-X}-Pb_X glasses, varying the Pb content.

X	E_1(ev)	σ_{ext}	E_2 (ev)	σ_{0loc}	B(ev)	σ_{0F}
0	0.992850483	0.087813788	0.898478715	0.085304823	0.981946487	0.039808917
10	0.134716464	0.036860109	0.118627281	0.038774919	0.106029803	0.030780091
20	0.123805895	0.048155948	0.12002239	0.03732086	0.120307103	0.019262379
30	0.733268895	0.165870488	0.729002952	0.135712218	0.623225927	0.129249731

To calculate the density of energy states we will determine the pre-exponential factor σ_o within these states. By plotting between DC conductivity and temperature, σ_o in these states' areas will be computed by assessing the range of these curves and their y-intercepts when the x-axis equals zero, according to equation 3. The values of σ_o have been computed and are presented in **Table (1)**. Utilizing the results derived from the continuous electrical conductivity versus temperature analysis in **Table (1)**, The density of energy states will be calculated theoretically by applying the equations in the three regions (local, extended, and Fermi).

3.1. Density of states in the extended state

Table (2) shows and according to the Mott and Davis method, the density related to the valence of extended states $N(E_v)$ and conduction $N(E_c)$ bands and that calculated by applying equation (9). **Figure (3)** shows the lead concentration and its relationship with the energy density in the extended states, which decreases with increasing the lead concentration due to the activation energy and the changes that occur in it, which are attributed to moving the Fermi level up or down or the change in width of these tails or in value of the gap mobility or in the concentration of carriers or the conversion in the conduction type n and p. Therefore, these reasons can affect the energy density in the three regions (16-20).

Table 2. Demonstrates the relationship between energy density in the three regions, R, (ΔE), as a function of the concentration of Pb in S_{60}-Se_{40-X}-Pb_X.

X	The width of tail ΔE (ev)	R(A^0)	a (A^0)	N (E_{ext}) ($ev^{-1}cm^{-3}$)	N (E_{loc}) ($ev^{-1}cm^{-3}$)	N (E_F) ($ev^{-1}cm^{-3}$)
0	0.094371768	2.492879285	1.151555396	4.53333E+24	3.21723E+21	9.85E+18
10	0.016089183	1.59901039	2.743411385	1.90288E+24	2.29462E+37	1.27E+17
20	0.003783505	0.429626116	2.099895134	2.48602E+24	5.20569E+37	2.04E+17
30	0.004265942	0.098048932	6.096469743	8.56296E+24	3.3086E+38	3.03E+18

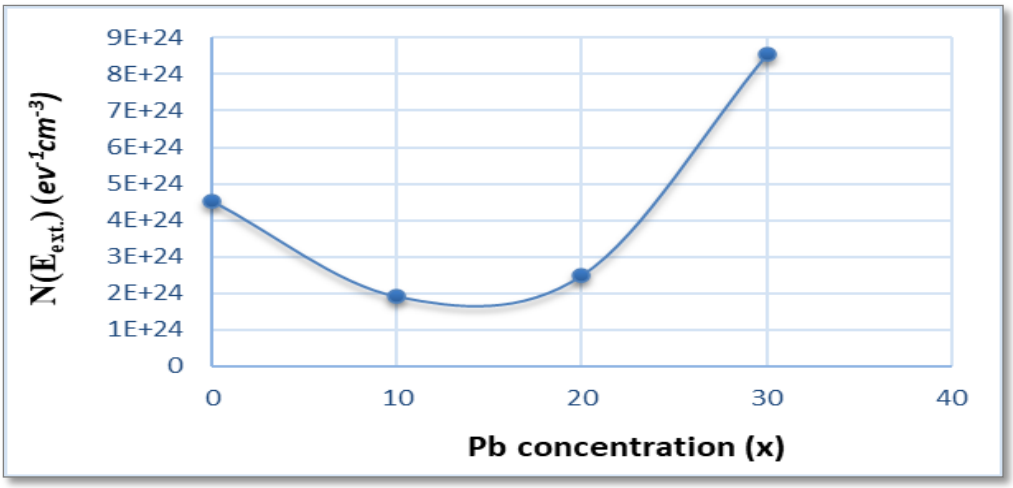

Figure 3. Extended states density in relation to the concentration of Pb for S_{60}-Se_{40-X}-Pb_X glasses with varying x values (0, 10, 20, and 30).

Using the equation a = 0.026 [e2/$\hbar\sigma_o$], interatomic distance (a) is calculated and the relationship between the Pb concentration and the interatomic distance (a) will be represented in **Figure (4**), which shows the direct relationship between them.

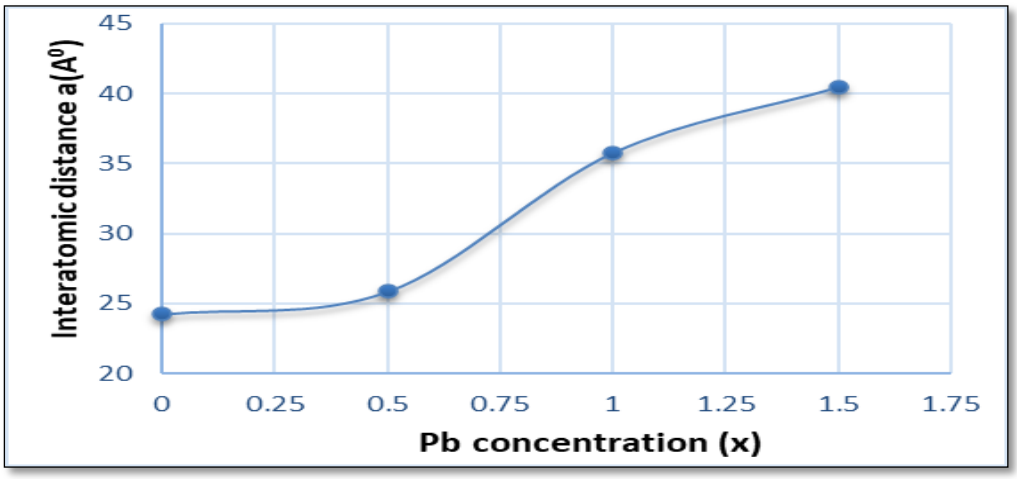

Figure 4. The distance of interatomic (a) in relation to the Pb concentration for S_{60}-Se_{40-X}-Pb_X glasses with varying x values (0, 10, 20, and 30).

3.2. Density of states in the localized state

In **Table (1)**, The results of the hopping distances of the localized charge carriers R were included after calculating them using equation (13). The results showed the inverse relationship between the lead concentration and the hopping distance, as the growing of the distance of hopping leads to a growth in the localized states density in the band of valence tail regions and the band

of conduction tail regions, where the hopping distance is expressed as the distance between two successive states of the localization levels that the carriers cross. The relationship between the lead concentration and the hopping distance will be shown in **Figure (5**), which shows an increase in the R values with Pb concentration.

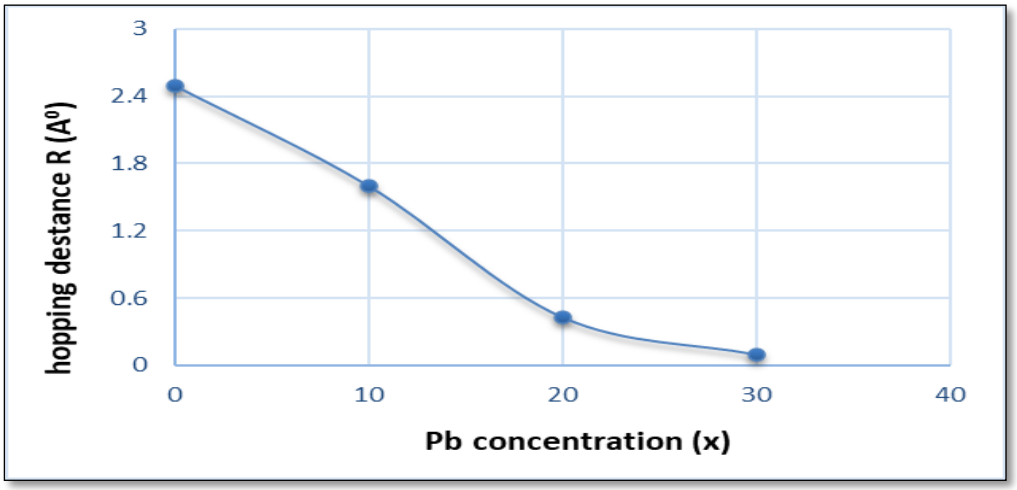

Figure 5. The hopping distance in relation to the concentration of lead.

The follow equation $\Delta E = E_1 - E_2$ represent the relationship between the lead concentration and the width of the tail of energy, as shown in **Figure (6**), which shows a decrease in the tail width ΔE values with an increase in the concentration of the lead x, and then a slight increase in the tail is observed when the lead concentration x is 30.

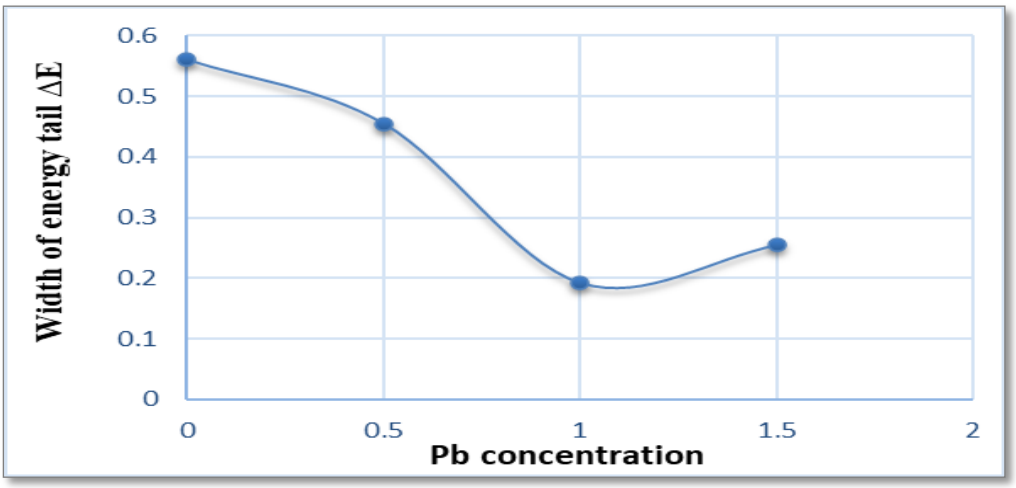

Figure 6. The lead concentration in relation to energy tail width.

The results of the density of the localized states energy $N(E_{loc})$ were listed in **Table (2)**, which were calculated by calculating the hopping distance between electrons, which is denoted by R, as well as by calculating the width of the energy tail by the equation $\Delta E = E_1 - E_2$ and substituting these values with the values of the photon frequency V_{ph} and the values of the pre-exponential factor σ_{0loc} in equation 12. This table, which is represented in **Figure (7**), shows that with the increase in the percentage and concentration of lead in the samples, the density of these states increases, which was interpreted on the basis that the introduction of Pb leads to narrow tails and thus reduces the crystal structure randomness of the S_{60}-Se_{40-X}-Pb_X compound and then lead to an increase in the state density at this region.

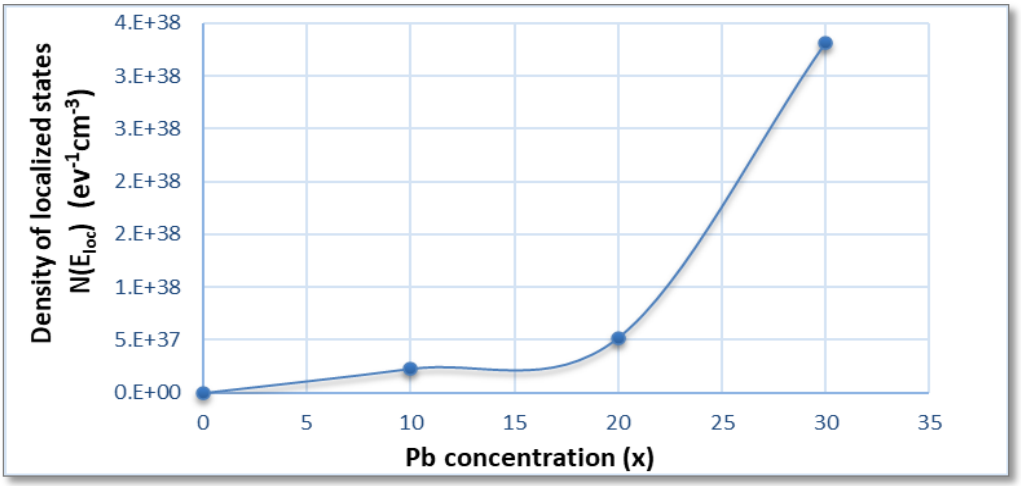

Figure 7. depicts the $N(E_{loc})$ in relation to the concentration of Pb for S_{60}-Se_{40-X}-Pb_X glasses with varying x values (0, 10, 20, and 30).

3.3. The Density in the Fermi level states

Table (2) shows at the Fermi level, the localized state density $N(E_F)$, calculated using equations 16 or 17 with specific parameters, and **Figure (8)** shows the $N(E_F)$ relationship with the lead concentration and that it indicates a decrease in $N(E_F)$ with increasing lead concentration.

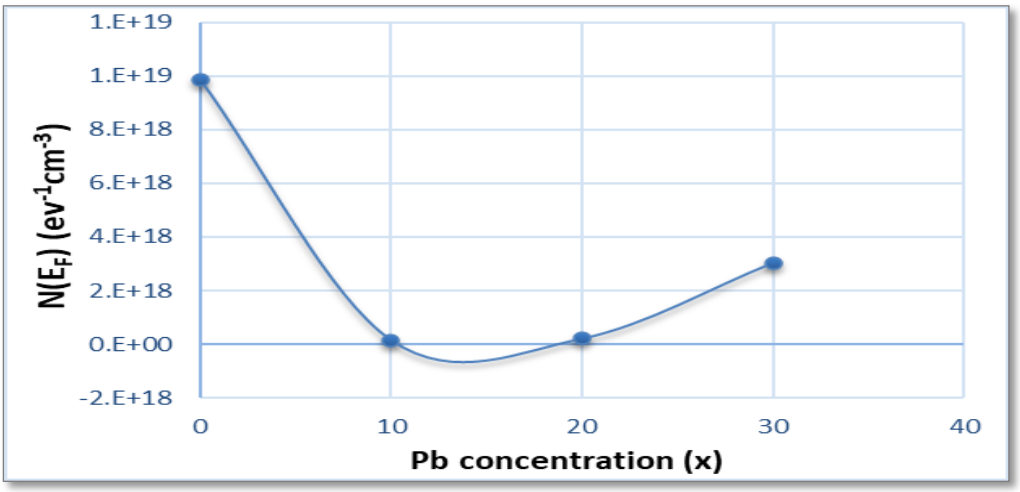

Figure 8. The $N(E_F)$ variation with the concentration of Pb for S_{60}-Se_{40-X}-Pb_X glasses with varying x values (0, 10, 20, and 30).

Within the extended region, the increased electronic state density implies that lead contributes to the creation of new electronic states, particularly in the conduction band, which is crucial for improving conductivity. This addition affects both extended and localized states, as well as the Fermi levels, across low, medium, and high temperatures (21-24). Within the localized region and in specific circumstances at moderate temperatures, augmenting the proportion of lead or substituting it in the S_{60}-Se_{40-X}-Pb_X samples has led to an increase in the state density, this increase leads to narrow tails and thus reduces the crystal structure randomness of the S_{60}-Se_{40-X}-Pb_X compound (25-27). Shifting in the Fermi level can occur when an increase in the ratio of the lead in the samples then affects the structure of the material in a way that reduces the density of states at the Fermi level and also modifies the alignment of energy levels within the material redistributing the states and reducing the density of states at the Fermi level (28-30).

4. Conclusion

Chalcogenides, which include elements from the chalcogen group (such as sulfur, selenium, and tellurium), exhibit unique electrical and optical properties that vary with their composition. The addition of lead can enhance the density of states in the energy band, potentially improving conductivity in certain regions while simultaneously reducing disorder and enhancing structural organization within the crystal lattice. At the (extended, local, and Fermi level) regions, the conductivity of D.C electrical changes in the chalcogenide alloy S_{60}-Se_{40-X}-Pb_X were studied by partial replacement of selenium with lead at variable ratios of X (0, 10, 20, and 30). The conduction mechanisms and their equations were explored and the electrical results of the conductivity and its effect on the energy density of these three regions.

Electrical assessments unveiled three mechanisms of conduction: extended state at high temperatures, local state at moderate temperatures, and (VRH) at low temperatures. The inclusion of Pb influenced a reduction in the density of Fermi states, the width of the energy tail ΔE, and the hopping distance between states (R). Pb additives contributed to an increase in the state's densities of extended and local regions, as well as the distance of interatomic.

Within the localized region, the addition or substitution of lead in the S_{60}-Se_{40-X}-Pb_X compound led to a decrease in state density, resulting in narrower tails and a subsequent reduction in disorder within the crystal structure. The presence of lead could interact with or suppress specific localized states in the material, thereby decreasing the state density

associated with these particular energy levels. The introduction of lead might shift the Fermi level or influence the material's band structure, ultimately reducing the stats of the Fermi level density. Practical applications of these chalcogenide alloys include their use in solar cells, where improved conductivity can lead to increased energy conversion efficiency, and in sensor technology, where their electrical properties can be tuned for specific environmental detections.

Acknowledgment

This article expresses my gratitude and appreciation to the College of Education for Pure Sciences, Ibn Al-Haytham, University of Baghdad, for their support in completing this work. Special thanks to the Physics Department for providing the necessary scientific facilities to aid in the success of this research project.

Conflict of Interest

This research was conducted with full transparency and integrity and the authors declare that they have no conflicts of interest."

Funding

None.

References

1. Chillab RK, Jahil SS, Wadi KM, Jasim KA, Shaban AH. Fabrication of Ge30Te70–xSbX glasses alloys and studying the effect of partial substitution on DC electrical energy parameters. Key Eng Mater. 2021 Oct 20;900:163–71. https://doi.org/10.4028/www.scientific.net/KEM.900.163.
2. Jasim KA, Hussein HS, Aneed SH, Salman EM. Examination of the Impact of Substituting Germanium for Bismuth on the Energy Density and Electrical Conductivity of the Se60Ge40–xBix Alloy. Korean J Mater Res. 2024;34(6):267–74. https://doi.org/10.3740/MRSK.2024.34.6.267.
3. Abd Al-hadi Z, Jasim KA. The Effect of Partial Substitution of Ge-S-Cd Alloys on the Density of Energy States. Ibn Al-Haitham J Pure Appl Sci. 2024 Jan 20;37(1):140–147. https://doi.org/10.30526/37.1.3314.
4. Davis EA. Non-crystalline materials. Endeavour. 1977 Jan 1;1(3–4):103–106. https://doi.org/10.1016/0160-9327(77)90167-3.
5. Liu YK, Zapien JA, Shan YY, Geng CY, Lee CS. Wavelength-controlled lasing in ZnxCdl−xS single-crystal nanoribbons. Adv Mater. 2005;17(11):1372–1377. https://doi.org/10.1002/adma.200401606.
6. Seddon AB. Chalcogenide glasses: a review of their preparation, properties and applications. J Non-Cryst Solids. 1995 May 1;184:44–50. https://doi.org/10.1016/0022-3093(94)00686-5.
7. Soltan AS, Moharram AH. Electrical switching in the chalcogenide As60–xTe40Cux glasses. Phys B Condens Matter. 2004;349(1–4):92–99. https://doi.org/10.1016/j.physb.2004.01.155.
8. Kumar S, Hussain M, Zulfequar M. Optical and other physical characteristics of amorphous Se-Te-Sn alloys. Physica B. 2006;371:193. https://doi.org/10.1016/j.mssp.2015.05.005.
9. Abdulateef NA, Alsudani A, Chillab RK, Jasim KA, Shaban AH. Calculating the mechanisms of electrical conductivity and energy density of states for Se85Te10Sn5–xInx glasses. J Green Eng. 2020;10(9):5487–5503.
10. Ahmed BA, Mohammed JS, Fadhil RN, Jasim KA, Shaban AH, Al Dulaimi AH. The dependence of the energy density states on the substitution of chemical elements in the Se6Te4–xSbx thin film. Chalcogenide Lett. 2022;19(4):301–308. https://doi.org/10.15251/cl.2022.194.301.
11. Juejun H, Xiaochen S, Agarwal AM, Viens JF, Kimerling LC, Petit L, et al. Studies on structural, electrical, and optical properties of Cu-doped As–Se–Te chalcogenide glasses. J Appl Phys. 2007;101(6):063520. https://doi.org/10.1063/1.2712162.

12. Jasim KA, Naser RF. The effects of micro-aluminum fillers in epoxy resin on the thermal conductivity. J Phys Conf Ser. 2018;1003(1):012082. https://doi.org/10.1088/1742-6596/1003/1/012082.
13. Gonçalves AP, Lopes EB, Delaizir G, Godart C. Semiconducting glasses: a new class of thermoelectric materials. AIP Conf Proc. 2012. https://doi.org/10.1063/1.4731568.
14. Zhao L, Wang X, Fei FY, Wang J, Cheng Z, Dou S, et al. High thermoelectric and mechanical performance in highly dense Cu2−xS bulks prepared by a melt-solidification technique. J Mater Chem A. 2015. https://doi.org/10.1039/C5TA01667C.
15. Biswas D, Singh YB, Hazra SK, Ghosh BK, Das AS, Mondal R, . Influence of Sb doping on thermal properties and electrical conductivity mechanism of SbxSe50–xSn20Te30 chalcogenide glassy systems. J Non-Cryst Solids. 2024 Jun 1;633:122953. https://doi.org/10.1016/j.jnoncrysol.2024.122953.
16. Huang PY, Kurasch S, Alden JS, Shekhawat A, Alemi AA, McEuen PL. Imaging atomic rearrangements in two-dimensional silica glass: watching silica's dance. Science. 2013;342:3–6. https://doi.org/10.1126/science.1242248.
17. Ellote SR. Electrical conduction mechanism in Se90–xTe5Sn5Inx (x=0, 3, 6, and 9) multi-component glassy alloys. AIP Adv. 2015;5:087164. https://doi.org/10.1063/1.4929577.
18. Cohen MH, Fritzsche H, Ovshinsky SR. Simple band model for amorphous semiconducting alloys. Phys Rev Lett. 1969;22:1065. https://doi.org/10.1103/PhysRevLett.22.1065.
19. Khudhair NH, Jasim KA. Preparation and study the effect of Sb on the energy density of states of Se60Te40. In: Technologies and Materials for Renewable Energy, Environment and Sustainability (TMREES22Fr); 2023. https://doi.org/10.1063/5.0129550.
20. Street RA, Mott NF. States in the gap in glassy semiconductors. Phys Rev Lett. 1975;35:1293–6. https://doi.org/10.1103/PhysRevLett.35.1293.
21. Mauro JC, Loucks RJ, Varshneya AK, Gupta PK. Enthalpy landscapes and the glass transition. Lect Notes Comput Sci Eng. 2009;68. https://doi.org/10.1007/978-1-4020-9741-6_15.
22. Kadhim BB, Risan RH, Shaban AH, Jasim KA. Electrical characteristics of nickel/epoxy-unsaturated polyester blend nanocomposites. AIP Conf Proc. 2019;2062. https://doi.org/10.1063/1.5116989.
23. Li Y, Zhong Y, Xu L, Zhang J, Xu X, Sun H. Ultrafast synaptic events in a chalcogenide memristor. Sci Rep. 2013;3:1619. https://doi.org/10.1038/srep01619.
24. Khudhair NH, Jasim KA. A study of the effectiveness of tin on the thermal conductivity coefficient and electrical resistance of Se60Te40–xSnx chalcogenide glass. Ibn Al-Haitham J Pure Appl Sci. 2023 Jan 20;36(1):149–157. https://doi.org/10.30526/36.1.2892.
25. Elliott GR, Murugan GS, Wilkinson JS, Zervas MN, Hewak DW. Chalcogenide glass microsphere laser. Opt Express. 2010;18(25):26720–26727. https://doi.org/10.1364/OE.18.026720.
26. Hegab NA, Afifi MA, Atyia HE, Farid AS. AC conductivity and dielectric properties of amorphous Se80Te20–xGex chalcogenide glass film compositions. J Alloys Compd. 2009 May 27;477(1–2):925–930. https://doi.org/10.1016/j.jallcom.2008.11.129.
27. Pattanayak P, Asokan S. Signature of a silver phase percolation threshold in microscopically phase-separated ternary Ge0.15Se0.85–xAgx (0≥x≥0.20) glasses. J Appl Phys. 2005;97(1):13–16. https://doi.org/10.1063/1.1827341.
28. Mohammed LA, Neamah ZJ, Watan AW, Jasim KA, Shaban AH. Determination of continuous electrical conductivity parameters and their influence on partial replacement of antimony with Sn in the Ge20Te72In8 chalcogenide glass. Int J Nanoelectron Mater. 2024 Jul 12;17(3):323–326. https://doi.org/10.58915/ijneam.v17i3.1012.
29. Frumar M, Wagner T. Ag-doped chalcogenide glasses and their applications. Curr Opin Solid State Mater Sci. 2003;7(March):117–26. https://doi.org/10.1016/S1359-0286(03)00044-5.
30. Jain Y, Kurchania R. Pressure-induced band gap enhancement and temperature-dependent thermoelectric characterization of semiconducting Transition Metal Chalcogenides LiMS (M = Cu, Ag). Mater Sci Semicond Process. 2025;186:109030. https://doi.org/10.1016/j.mssp.2024.109030.